The Rydberg states of NO_2: Vibrational autoionization of the $nd\sigma$ states

Ioannis D. Petsalakis and Giannoula Theodorakopoulos
Theoretical and Physical Chemistry Institute, The National Hellenic Research Foundation, 48 Vassileos Constantinou Avenue, Athens 116 35, Greece

Mark S. Child
Physical and Theoretical Chemistry Laboratory, Oxford University, South Parks Road, Oxford 0X1 3QZ, England

(Received 25 July 2001; accepted 11 September 2001)

Ab initio configuration interaction calculations were carried out on the potential-energy surfaces of the ground and Rydberg excited electronic states of NO_2. The results show that potential-energy curves with typically Rydberg form are obtained for most of the excited states at linear geometries, similar to the ground-state potential of NO_2^+. At nonlinear geometries valence-Rydberg interactions complicate the potential-energy surfaces of the excited states. Quantum defect functions have been determined from the *ab initio* results on the $3d\sigma$ Rydberg state and vibrational autoionization widths have been calculated for excited vibrational levels of members of the $nd\sigma$ series. © *2001 American Institute of Physics.* [DOI: 10.1063/1.1415084]

I. INTRODUCTION

The NO_2 radical has served as prototype in studies of state-to-state autoionization dynamics by high resolution laser spectroscopic methods-giving information on the higher excited Rydberg states of NO_2, vibrational autoionization of the Rydberg states and on the rotational-vibrational structure of the cation.[1–7] In these experiments, the Rydberg states of NO_2 serve as the intermediate states for the production of low-lying vibrational states of NO_2^+. A general framework for the theoretical treatment of vibrational autoionization in polyatomic molecules has been proposed[8] while vibrational autoionization widths in NO_2 have been calculated by an *ab initio* Fermi-Golden rule calculation.[9]

A comprehensive treatment of the autoionization dynamics in NO_2 is possible in the context of multichannel quantum defect theory (MQDT) once the appropriate quantum defect surfaces have been generated. *Ab initio* potential-energy surfaces of the lower-lying Rydberg states and the electronic states of the cation, which are the ionic limits of the Rydberg series, can serve in the determination of the quantum defect surfaces.[10,11] However, it is rather difficult to calculate accurately the potential-energy surfaces of the excited states for this 23-electron system. Even for the ground state, the symmetry breaking problem is difficult to resolve. The Rydberg states are, in principle, easier to calculate than valence states, since to a good approximation they may be described by a closed shell NO_2^+ core plus a Rydberg electron. The minimum energy geometry of the Rydberg states is expected to be linear and similar to the ground-state geometry of the cation core. The experimental geometry of the ground electronic state of NO_2 is a bent symmetric structure with a bond angle of 134.07° and bond length of 1.1934 Å.[12] At the ground-state geometry most of the lower-lying excited states are valence and favor bent geometries,[13] while the Rydberg states are very high in energy.

An early theoretical study[14] of the potential-energy surfaces of a large number of excited states of NO_2 provides a great deal of information on the electronic structure of this system but since diffuse functions were not included in the basis sets, the above study is not appropriate for the Rydberg states. Vertical transition energies to Rydberg states, at the experimental ground-state geometry have been obtained by previous configuration interaction calculations.[15] However there exists no report on the potential-energy surfaces of the Rydberg states of NO_2, such as would be required for an MQDT treatment of the highly excited Rydberg states and the vibrational autoionization of NO_2.

In the present work, *ab initio* multireference single and double substitutions configuration interaction (MRDCI) calculations[16,17] have been carried out on Rydberg states of the NO_2 radical, at symmetric linear and bent geometries and asymmetric linear geometries. The object of the present work is to calculate the potential-energy surfaces of the lower Rydberg states, which may serve to generate *s*, *p*, and *d* quantum defect surfaces, by combining the present calculations with the earlier reported potential-energy surface of the ground electronic state of the cation, NO_2^+ (Ref. 18) and to calculate autoionization widths of excited vibrational levels of the *nl* states.

The vibrational autoionization calculations were performed by using matrix elements of the quantum defect functions, in the NO_2^+ vibrational basis, to construct the MQDT K matrix. Standard MQDT theory was then employed to calculate ion yield profiles, as a function of photon energy, for double resonance excitation via several vibrational levels of the $3p\ ^2\Sigma_u^+$ Rydberg state.

II. *AB INITIO* MRDCI CALCULATIONS

Ab initio MRDCI calculations have been carried out on *s*, *p*, and *d* Rydberg electronic states of NO_2. Most of the

calculations have been carried out in C_{2v} symmetry as it is common to bending, symmetric stretch, and linear asymmetric stretch geometries. One set of calculations, involving linear symmetric geometries ($D_{\infty h}$ symmetry), corresponding to symmetric stretch displacements, has been also carried out in D_{2h} symmetry, since in this higher symmetry (than C_{2v}) it is possible to distribute the electronic states into different CI calculations, corresponding to the different irreducible representations. In this manner it is easier to identify the states and to calculate them with higher accuracy.

The atomic orbital basis set is basically as in the calculations on NO_2^+[18] consisting of the $[11s6p/5s3p]$ basis sets of Dunning[19] for oxygen and nitrogen, where the nitrogen basis set was augmented for the present calculations with *s*, *p*, and *d* diffuse functions, with exponents 0.028, 0.0066, and 0.0032 for the *s*, 0.025 and 0.0051 for the *p*, and 0.015 and 0.0032 for the *d* functions. For most of the calculations, a single *d* polarization function with exponent 0.88 was included in both the oxygen and the nitrogen basis sets. A set of test calculations in C_{2v} symmetry employing two *d* polarization functions with exponents 1.5 and 0.38 in each AO basis set, showed that it is sufficient to employ the single *d* polarization basis sets.

In the linear symmetric geometry the ground state of NO_2 is $^2\Pi_u$ which is calculated as $1^2B_{2u}+1^2B_{3u}$ in D_{2h} symmetry ($1^2A_1+1^2B_1$ in C_{2v}). The Rydberg states in the linear geometry, are calculated as follows: *s* ($^2\Sigma_g^+$) as ^2A_g, *p* ($^2\Sigma_u^+$,$^2\Pi_u$) as $^2B_{1u}$ and $^2B_{2u}+^2B_{3u}$ respectively, and *d* ($^2\Sigma_g^+$,$^2\Pi_g$ and $^2\Delta_g$) as ^2A_g, $^2B_{2g}+^2B_{3g}$ and $^2A_g+^2B_{1g}$, respectively. In the present calculations, seven ^2A_g, six $^2B_{1u}$, six $^2B_{2u}$ and two $^2B_{3g}$ states. Large reference spaces of the order of 100 configurations in each case, determined on the basis of preliminary calculations at different linear symmetric geometries, have been employed and selection of configurations were carried out with respect to the above roots and a threshold of 1×10^{-6} Hartree.

In bent geometries the point group symmetry of the molecule is C_{2v} and the ground state is $X\ ^2A_1$. At linear geometries the C_{2v} states correlate with the linear as follows: $^2A_1\rightarrow{}^2\Sigma_g^+$, $^2A_1+^2B_1\rightarrow{}^2\Pi_u$, and $^2\Delta_g$, $^2B_2\rightarrow{}^2\Sigma_u^+$, $^2B_2+^2A_2\rightarrow{}^2\Pi_g$, etc. In this symmetry, nine $^2A_1$, five $^2B_1$, six $^2B_2$, and four $^2A_2$ states have been calculated at geometries ranging in bond angle from 120° to 180° and N–O bond lengths from 1.8 to 2.7 bohr. Reference spaces of 68, 46, 56, and 54 configurations for the above symmetries respectively and selection thresholds of 2×10^{-6} Hartree for the $^2A_1$, and 1×10^{-6} Hartree for the other symmetries were employed. The resulting CI spaces range from 100 000 to 200 000 configurations, over the different geometries.

A second set of C_{2v} calculations have been carried out on linear asymmetric geometries, corresponding to antisymmetric stretch and to asymmetric dissociation with one of the N–O bond lengths fixed at 2.12 bohr. These calculations involved $^2A_1$ ($^2\Sigma$ and $^2\Delta$) and $^2B_1$ ($^2\Pi$) states, with reference spaces of 87 and 86 configurations and selection thresholds of 2×10^{-6} Hartree for the $^2A_1$, and 1×10^{-6} Hartree, respectively.

III. RESULTS OF THE *AB INITIO* CALCULATIONS

A. Results of the D_{2h} calculations: Symmetric stretch potentials

At the equilibrium geometry of the ground state of the cation, i.e., linear symmetric geometry with N–O bond lengths of 2.1203 bohr, all the lower-lying excited states of NO_2 have Rydberg character. At longer bond lengths, starting at N–O of 2.15 bohr, the first excited state $1^2\Sigma_g^+$ becomes valence, while at even larger bond lengths there are avoided crossings of the Rydberg with the valence states: The linear symmetric stretch potentials of the electronic states of NO_2 along with the stretching potential of the ground state of NO_2^+ have been plotted in Figs. 1(a)–1(d). As shown in Fig. 1(a), the ground state $X^2\Pi_u$ favors a longer bond length than the cation, whereas the stretching potentials of the two Rydberg states $3p$ and $4p$ $2\ ^2\Pi_u$ and $3\ ^2\Pi_u$ follow closely the shape of the ground-state potential of the cation. At large bond lengths, there is a valence-Rydberg interaction causing an avoided crossing with valence states, which at short bond lengths lie higher in energy than the ground state of the cation. A similar situation is encountered with the stretching potentials of the $3p$ and $4p$ $1\ ^2B_{1u}$ and $2\ ^2B_{1u}$ ($1\ ^2\Sigma_u^+$ and $2\ ^2\Sigma_u^+$) states, see Fig. 1(b), which also show valence-Rydberg interactions, again manifested as avoided crossings at large bond lengths with higher-lying valence states. These valence-Rydberg interactions may lead to predissociation of the Rydberg states.

The calculated energies of the ^2A_g states have been plotted in Fig. 1(c). As shown, the Rydberg states follow the potential of the cation, in that the minimum is at the same value of N–O bond length as in the potential of the cation. However, the lowest ^2A_g state ($1\ ^2\Sigma_g^+$), which at short *R* has Rydberg 3_s character, changes from Rydberg to valence at N–O larger than 2.15 bohr, with a minimum at 2.45 bohr. The change in character here occurs at the molecular orbital level and it is not a consequence of an avoided crossing with a valence state. Similarly, the symmetric stretch potential of the $2\ ^2A_g$ 4s state ($2\ ^2\Sigma_g^+$) and that of the $5\ ^2A_g$ 5s state ($4\ ^2\Sigma_g^+$), at bond lengths larger than the minimum energy value, deviate from the potential of the cation, as they take on the character of the lower state, i.e., 3s and 4s, respectively. The symmetric stretch potentials of the 3d, $3\ ^2A_g$, and $4\ ^2A_g$ ($3\ ^2\Sigma_g^+$ and $1\ ^2\Delta$), and $4d$, $6\ ^2A_g$ and $7\ ^2A_g$ ($4\ ^2\Sigma_g^+$ and $2\ ^2\Delta$) states [cf. Fig. 1(c)] and those of the 3d and 4d $^2\Pi_g$ [Fig. 1(d)] do follow closely the corresponding potential of the cation. As shown in Figs. 1(c) and 1(d), in the case of the *s* and *d* Rydberg states, the valence-Rydberg interactions do not lead to dissociation, at least in the symmetric stretch coordinate.

B. Results of the C_{2v} calculations: Asymmetric linear geometries

The results of the calculations on linear asymmetric geometries are summarized in Figs. 2(a)–2(d). As shown [Figs. 2(b) and 2(d)], the electronic states of NO_2 are bound with-

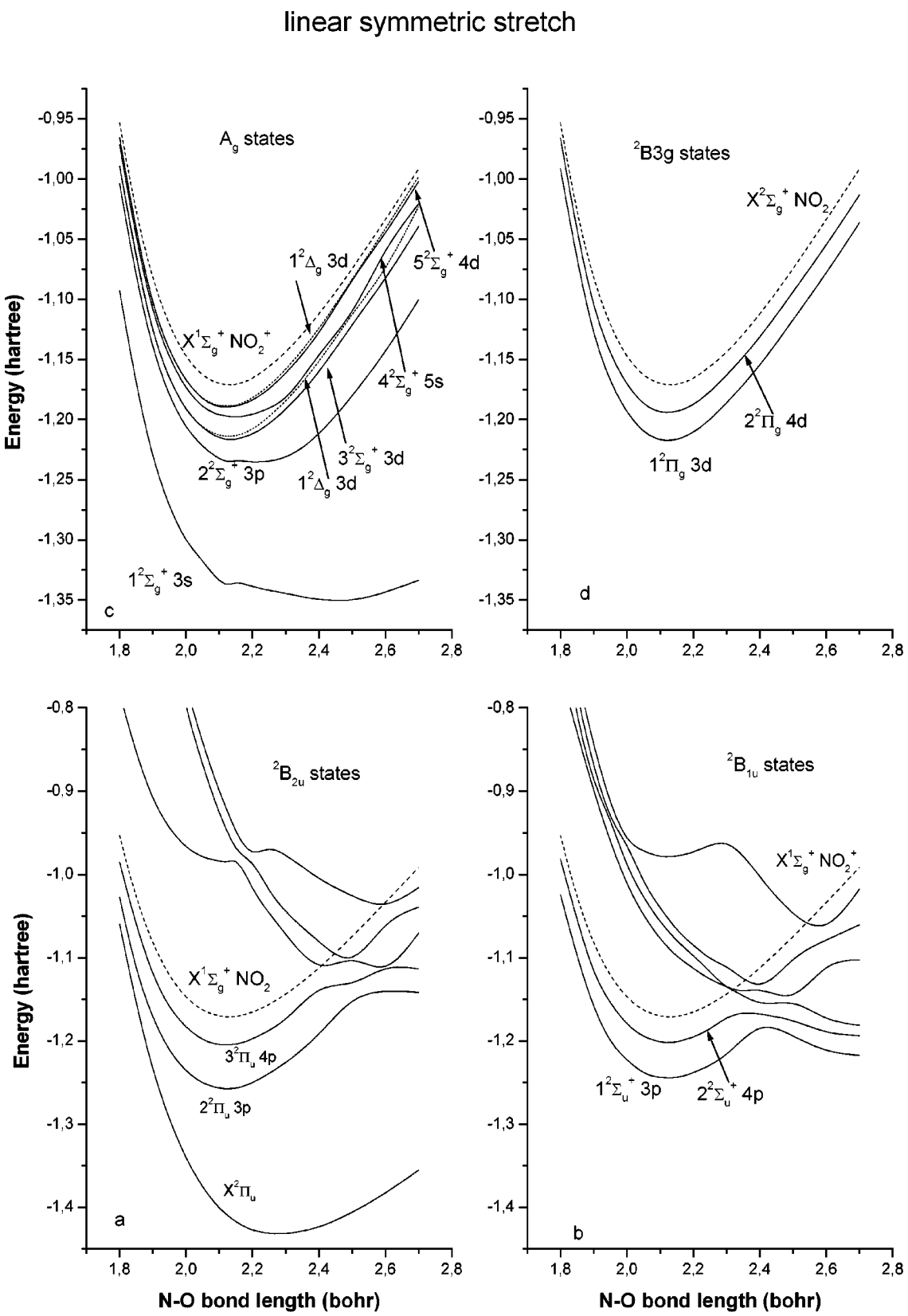

FIG. 1. Symmetric stretch potentials, results of D_{2h} calculations: (a) $^2B_{2u}$ states, (b) $^2B_{1u}$ states, (c) A_g states, (d) $^2B_{3g}$ states.

respect to antisymmetric stretch, at least for the displacements considered. The calculations along the asymmetric dissociation path show that the lowest $^2\Sigma^+$ state is dissociating [Fig. 2(a)] while the Rydberg $^2\Sigma^+$ states have maxima at the long N–O distance ($N–O_{(2)}$) near 2.6–2.8 bohr, which result from valence-Rydberg interactions and become dissociating at larger distances. The $^2\Delta$ states [dotted lines in Fig. 2(c)] and the $^2\Pi$ states [Fig. 2(c)] seem to be stable with

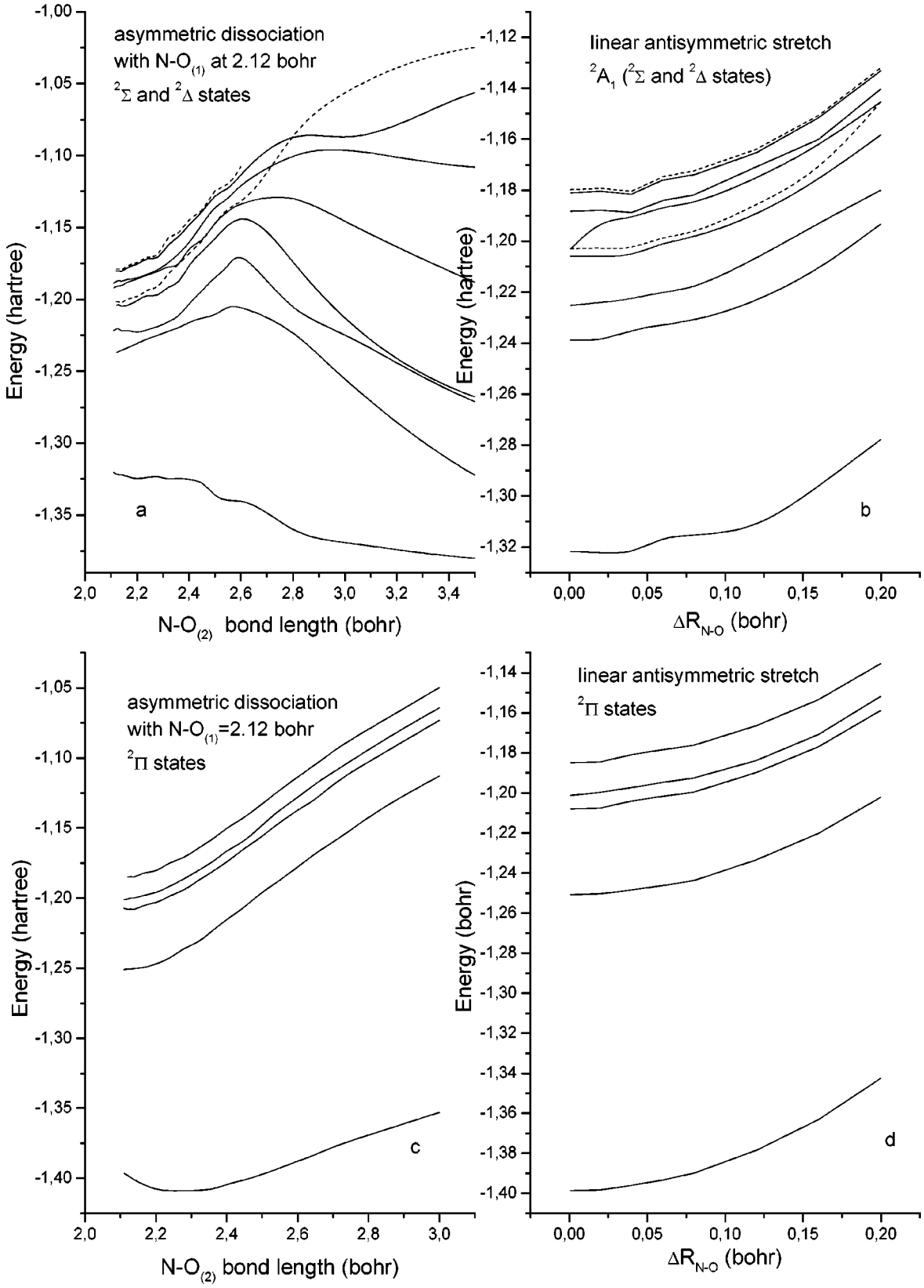

FIG. 2. Linear asymmetric dissociation and linear antisymmetric stretch: (a),(b) $^2\Sigma$ and $^2\Delta$ states, (c),(d) $^2\Pi$ states.

respect to asymmetric dissociation. It might be noted however that it was not possible to calculate the $^2\Pi$ states for the geometries with the long N–O distance larger than 3.0 bohr [Fig. 2(d)]. Thus, it is conceivable that, beyond that point, a large change occurs in the character of the states caused by possible avoided crossings with valence states, and it is no longer possible to calculate them with the reference set employed.

C. Results of the C_{2v} calculations: Bending potentials

Bending potentials have been calculated at different values of the N–O bond length, ranging from 1.8 to 2.7 bohr. The complete set of calculated energies may be obtained directly from the authors.

The bending potentials at N–O bond length of 2.1203 bohr, which is the equilibrium bond length of the cation NO_2^+ and of the Rydberg states and at N–O of 2.2552 bohr, which is the equilibrium bond length of the $X\ ^2A_1$ of NO_2, are collected in Figs. 3(a)–3(f). All the excited $^2A_1$ states favor linear geometry, as may be seen in Figs. 3(a) and 3(b). The ground state, $X\ ^2A_1$, has minimum at a bond angle of 134°, and for bond length of 2.2552 bohr [Fig. 3(b)] the whole curve is shifted to lower energies than at bond length of 2.1203 bohr [Fig. 3(a)]. Conversely, the bending potentials of the higher $^2A_1$ excited states shift to higher energies at N–O bond length of 2.2552 bohr. The bending potentials of the first excited $^2A_1$ state at 2.1203 and 2.2552 bohr are very close, while at linear geometry, the longer bond length is favored. The bending potentials of the second and especially the third excited $^2A_1$ states at 2.2552 bohr, for bond angles smaller than 140° turn towards lower energies, indicating the existence of a minimum at small bond angles.

The bending potentials of all the $^2B_1$ states show a minimum at the linear geometry, as shown in Figs. 3(c) and 3(d). The lowest $^2B_1$ state ($A\ ^2B_1$) meets $X\ ^2A_1$ at 180° where the two states give $X\ ^2\Pi_u$. Again, at bond lengths of 2.2552 bohr [Fig. 3(d)] the bending potential of the $A\ ^2B_1$ state shifts to lower energies while those of the Rydberg $^2B_1$ states shift to higher energies, especially near bond angle of 180°. It might be noted that in the C_{2v} calculations slightly higher energies are calculated than in the D_{2h} calculations, while at 180° the calculated energies of the $X\ ^2A_1$ and $A\ ^2B_1$ states are not identical. It is rather difficult to accommodate simultaneously the various valence and Rydberg states (of the same symmetry) and to calculate the electronic states with similar accuracy over the different geometries. A large number of roots must be included in order to account for all the relevant states and their interactions, which makes the calculation very large.

The bending potentials of the $^2B_2$ states are very complicated, cf. Fig. 3(e), showing the characteristic Rydberg shapes only for bond angles larger than 160° (at bond length of 2.1203 bohr) and series of valence-Rydberg interactions at smaller bond angles. At a bond length of 2.2552 bohr [dotted lines in Fig. 3(e)], the Rydberg region is restricted to angles very close to 180°. A similar picture is shown by the bending potentials of the $^2A_2$ states [cf. Fig. 3(f)]. The minima of the lower-lying valence $^2B_2$ and $^2A_2$ states are to be found at smaller bond angles than calculated here.[14] The present work is mainly concerned with the Rydberg states of NO_2 and thus the determination of the minima of the valence states at small bond angles has not been pursued. Information on the equilibrium conformation of the valence states exists elsewhere.[13,14]

D. Transition energies

In order to provide some comparison with previously calculated quantities and experimental data, vertical transition energies with respect to the ground state, at the ground-state experimental geometry, with N–O of 2.2552 bohr and ONO angle of 134.07° are listed in Table I. Generally good agreement is obtained with the available experimental data and with the results of previous calculations at the experimental geometry.[15]

As noted above, the attention of the present work is focused on the Rydberg states for which the region of importance for their spectroscopy is at linear geometries. The transition energies at the linear geometry and N–O of 2.1203 bohr are listed in Table II. As shown in Table II, the different C_{2v} states corresponding to degenerate states of linear symmetry are not calculated degenerate: the $^2B_1$ component of the $^2\Pi_u$ and the $^2\Delta_g$ states is calculated from 0.07 to 0.1 eV lower than the $^2A_1$. The 3p $1\ ^2\Sigma_u^+$ state, which serves as the intermediate linear state in the three-photon autoionization of NO_2, has experimental T_0 of 55 649.2 cm^{-1} (6.90 eV),[7] while the present theoretical adiabatic ΔE_{el} value is 6.53 eV, showing that the Rydberg states are treated better than the ground state. For the calculation of the quantum defect functions, it is required to have the correct energy difference between the Rydberg states and the corresponding ionic limit. The experimental adiabatic ionization potential is estimated at 77 315.9 cm^{-1} (9.59 eV),[5] which means an experimental energy difference between the 3p $1\ ^2\Sigma_u^+$ state and the ground state of the ion of about 21 667 cm^{-1} (2.69 eV). This value may be used to compare with the corresponding calculated energy difference and to shift uniformly the calculated potential-energy surfaces of all the Rydberg states accordingly, since there have not been reported experimental ionization energies for any of the other Rydberg states of NO_2. In this manner the quantum defect analysis which follows must be viewed in terms of its qualitative aspects.

IV. QUANTUM DEFECT CALCULATIONS: AUTOIONIZATION

From the calculated energies of the lower-lying Rydberg states, $E(Q)$ and the potential-energy surface of the cation $V^+(Q)$, it is possible to generate quantum defect functions [Eqs. (10) and (11)]. Single-channel quantum defect functions $\mu_{il\lambda}(Q)$, where i refers to the ionic state and $l\lambda$ to the particular channel, may be calculated from

$$\tan\ \pi\mu_i(Q)+\tan\ \pi\nu_i(Q)=0, \tag{1}$$

where

$$\nu_i(Q)=[2(V_i^+(Q)-E(Q))]^{-1/2}. \tag{2}$$

As mentioned above the potential-energy surfaces of the excited states of NO_2 are complicated by valence-Rydberg or Rydberg–Rydberg (e.g., among the different nl states) interactions. The $3d\sigma$ state ($5\ ^2A_1$ state of the C_{2v} calculations) was found to be relatively free of such interactions for a region of molecular geometries near the equilibrium [cf. Figs. 1–3], so it is possible to calculate the single channel quantum defect function for this state. A functional expression for the resulting quantum defect function is obtained in terms of the symmetric displacement ΔR from the equilibrium bond length and the bond angle θ using

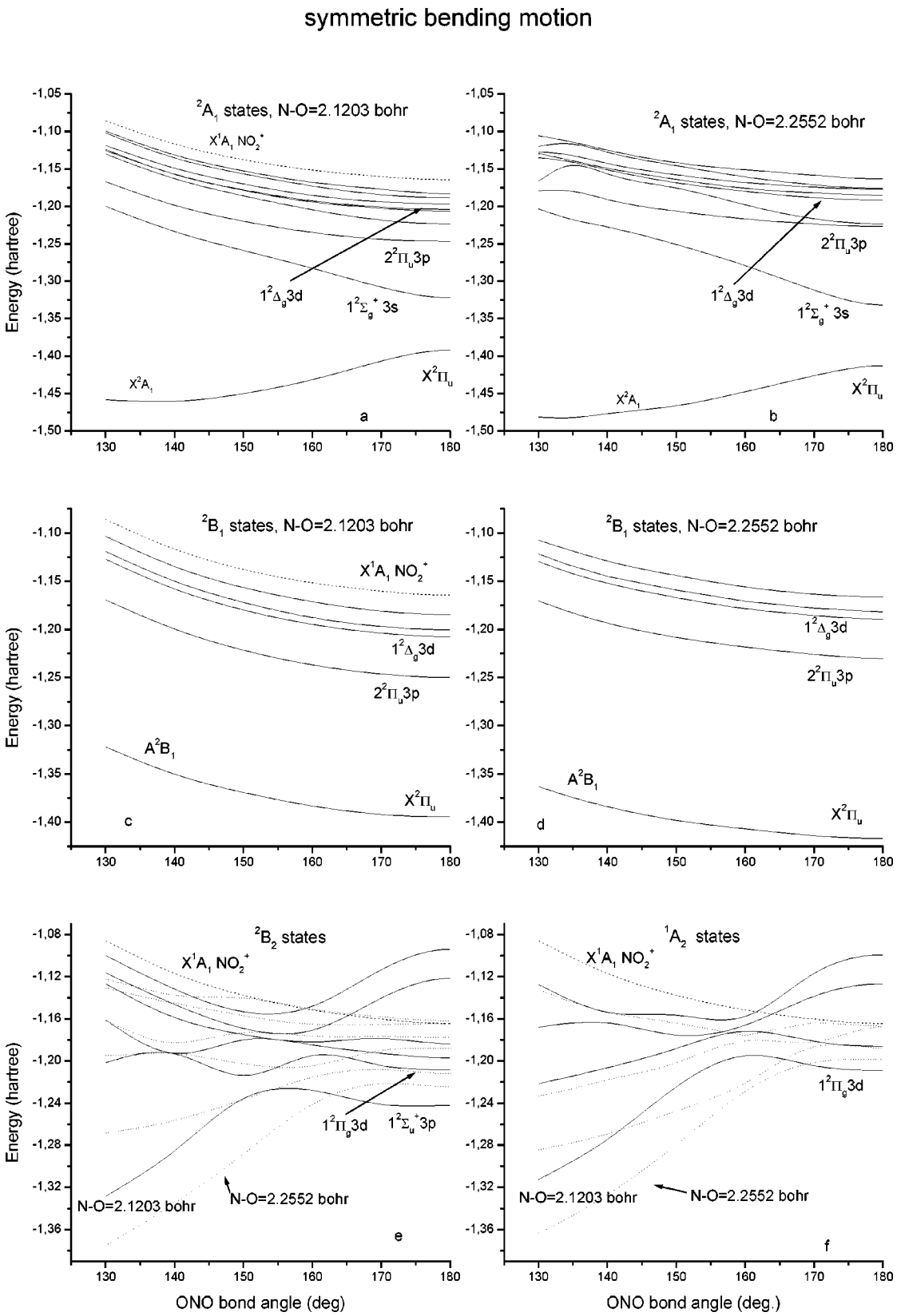

FIG. 3. Bending potentials: (a) $^2A_1$ states, $R_{N-O}=2.1203$ bohr, (b) $^2A_1$ states, $R_{N-O}=2.2552$ bohr, (c),(d) as in (a),(b) but for $^2B_1$ states, (e) $^2B_2$ states, solid lines for $R_{N-O}=2.1203$ bohr, dotted for $R_{N-O}=2.2552$ bohr, (f) as in (e) but for the $^2A_2$ states.

$$\mu(\Delta R,\theta)=\sum_{\substack{i=0\\ j=0}}^{2} C_{ij}\Delta R^i \cos\ \theta^{\,j}, \tag{3}$$

where $\Delta R=(R-R_e)$ and $R_e=2.103$ bohr and the coefficients are obtained by a least-squares fit to the *ab initio* μ values derived from Eqs. (1) and (2) at the *ab initio* energy points. The resulting coefficients for the $3d\sigma$ $(3\,^2\Sigma_g^+)$ state are listed in Table III.

TABLE I. Vertical transition energies (eV) with respect to the ground state, at the experimental ground-state geometry, 2.2552 bohr and 134.07° of NO_2.

State	Present work	Other theoretical[a]	Experimental[b]
$1\,^2B_2$	3.10	3.22, 3.03, 3.4, 2.43	2.9–3.0, 3.10
$1\,^2B_1$	2.83	2.79, 2.45, 2.8, 2.46	2.7–3.1, 2.81, 2.84
$1\,^2A_2$	3.39	3.25, 3.9, 3.4, 2.15	
$2\,^2A_2$	5.34	5.04, 4.14	5.28–6.2
$2\,^2B_2$	5.66	5.5, 5.8, 4.24	5.22
$3\,^2A_2$	6.71	6.76, 5.45	
$2\,^2A_1$	7.24	7.71, 6.59	6.2–7.52,[a] 7.5
$3\,^2B_2$	8.16	8.84, 7.38	
$2\,^2B_1$	8.17	8.62, 6.17	7.52–9.19, 8.6
$3\,^2A_1$	8.20	8.73, 7.20	
$4\,^2B_2$	8.22	8.29	
$4\,^2A_1$	9.14	9.75	
$4\,^2A_2$	9.24	9.74	
$3\,^2B_1$	9.27	7.93	
$5\,^2A_1$	9.28	11.65	
$6\,^2A_1$	9.31	12.12	
$5\,^2B_2$	9.06	9.18	
$4\,^2B_1$	9.49	8.16	9.66
$7\,^2A_1$	9.51	12.63	9.50–9.92
$6\,^2B_2$	9.68	9.70, 10.79	9.66
$5\,^2A_2$	9.93	9.86, 9.91	10.83–11.2 (9.75–10.05)
$5\,^2B_1$	9.90	12.21	
$8\,^2A_1$	9.88	13.79	
$9\,^2A_1$	10.01	16.02	

[a]From Refs. 14 and 15.
[b]From Refs. 12, 14, and 15.

The simplest case of vibrational autoionization involves coupling between the bound levels of a closed vibrational channel with the continuum of a lower vibrational state belonging to the same electronic channel, with quantum defect function $\mu_\alpha(Q)$ say, where $|\alpha\rangle = |il\lambda\rangle$. In the present calculations autoionization of manifolds of states, belonging to the $nd\sigma$ electronic channel and converging to higher vibrational levels of the cation, by a lower-lying threshold of the same vibrational symmetry, will be examined. For example autoionization of the (010) and the (001) manifolds by the (000) threshold, is symmetry-forbidden.

The first step in an MQDT autoionization calculation[11,20,21] is to construct a vibrational K matrix with elements

$$K_{\nu_-\nu_+} = \langle \nu_+ | \tan\ \pi\mu_\alpha(Q) | \nu'_+ \rangle, \tag{4}$$

where $|\nu_+\rangle$ are vibrational states of the positive ion. Application of the appropriate boundary conditions then leads to equations of the form[20]

$$\begin{pmatrix} K_{cc} + \tan\ \pi\nu(E), K_{cc} \\ K_{oc}, K_{oo} - \tan\ \pi\tau(E) I_{oo} \end{pmatrix} \begin{pmatrix} Z_c \\ Z_o \end{pmatrix} = 0, \tag{5}$$

where o and c denote open and closed channels, respectively. I_{oo} is the open channel unit matrix and $\tan\ \pi\upsilon(E)$ is a closed channel diagonal matrix such that

$$\nu_{\nu_+}(E) = \{R_y/(E_{\nu_+} - E)\}^{1/2}, \tag{6}$$

and $\tau(E)$ are the eigenphases, which are parameterized in the Breit–Wigner form

$$\tau(E) = \tau^o(E) + \pi^{-1}\ \arctan[\Gamma_r/2(E_r E)], \tag{7}$$

where E_r is the resonance position and Γ_t is the linewidth. In Eq. (5) Z_c and Z_o are the closed and open channel amplitudes, respectively. Equation (5) is commonly solved by using the closed portion to express the N_c closed channel amplitudes in terms of the N_o open channel ones; thus

$$Z_c = -[K_{cc} + \tan\ \pi\nu(E)]^{-1} K_{co} Z_o, \tag{8}$$

whereby Eq. (5) reduces at any energy to an $N_o \times N_o$ eigenvalue equation for $\tan\ \pi\nu(E)$. The corresponding open channel coefficients, $Z_o(E)$ determine the photoionization distribution over the open channels, while $Z_c(E)$ determine the spectroscopic lineshape profiles. The open channel coefficients are normalized such that

$$\sum_{i=\text{open}} (Z_i^\rho)^2 = \cos^2\ \pi\tau_\rho, \tag{9}$$

where the subscript ρ distinguishes different eigenphases if there are several open channels. Finally, to the extent that vibrational wave functions in the intermediate $3p\sigma$ electronic state are identical with those of the positive ion, the photoionization cross sections for intermediate excitation via

TABLE II. Transition energies (eV) of the Rydberg states at linear geometry with N–O=2.1203 bohr.

State	C_{2v} states	Energy (eV)
$X\,^2\Pi_u$	$X\,^2A_1$, $A\,^2B_1$	0.07, 0.00
$1\,^2\Sigma_g^+\ 3s$	$2\,^2A_1$	1.97
$2\,^2\Pi_u\ 3p$	$3\,^2A_1$, $2\,^2B_1$	4.03, 3.94
$1\,^2\Sigma_u^+\ 3p$	$1\,^2B_2$	4.15
$2\,^2\Sigma_g^+\ 4s$	$4\,^2A_1$	4.65
$1\,^2\Pi_g\ 3d$	$1\,^2A_2$, $2\,^2B_2$	5.05, 5.07
$3\,^2\Sigma_g^+\ 3d$	$5\,^2A_1$	5.11
$1\,^2\Delta_g\ 3d$	$6\,^2A_1$, $3\,^2B_1$	5.19, 5.09
$3\,^2\Pi_u\ 4p$	$7\,^2A_1$, $4\,^2B_1$	5.38, 5.28
$2\,^2\Sigma_u^+\ 4p$	$3\,^2B_2$	5.38
$4\,^2\Sigma_g^+\ 5s$	$8\,^2A_1$	5.61
$2\,^2\Pi_g\ 4d$	$2\,^2A_2$, $4\,^2B_2$	5.68, 5.74
$5\,^2\Sigma_g^+\ 4d$	$9\,^2A_1$	5.75
$2\,^2\Delta_g\ 4d$	$5\,^2B_1$	5.71

TABLE III. Global-fit single channel quantum defect function for the $^1A_1$ $nd\sigma$ state of NO_2.

C_{ij}[a]	$^1A_1 nd(^2\Sigma^+)$[b]
C_{00}	39.080 882
C_{01}	81.418 558
C_{02}	42.549 690
C_{10}	43.996 894
C_{11}	86.281 594
C_{12}	42.544 297
C_{20}	−65.662 40
C_{21}	−100.442 885
C_{22}	−35.873 229

[a]C_{ij} is the coefficient of the term $(\Delta R)^i(\cos\ \theta)^j$.
[b]Fit over region $2.0 < R < 2.4$ bohr, and $\theta = 160°$, 170°, 180° only.

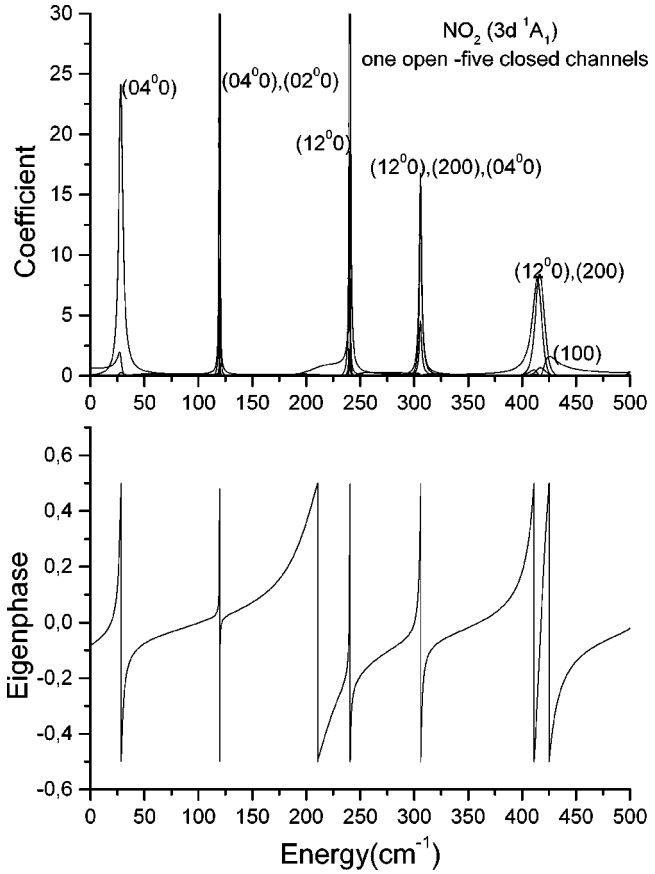

FIG. 4. Eigenphase as a function of the energy above the (000) level of NO_2^+ (lower part) and variation of the relative coefficients corresponding to the calculated levels (upper part). Nominal principal quantum numbers are $n=7$ for the (04^00), (12^00), and (200) levels, $n=10$ for (02^00) and $n=11$ for (100).

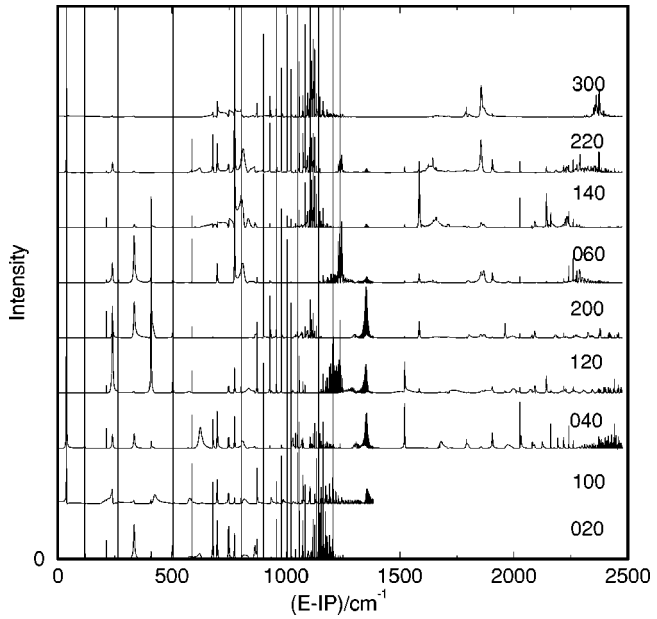

FIG. 5. Overview of the spectra corresponding to the nine lowest vibrational levels of the (000) manifold.

the vibrational state $|j\rangle$, the counterpart of which is necessarily closed in the autoionization region, are proportional to

$$X_j=\sum_{\rho}(Z_j^{\rho})^2, \tag{10}$$

where Z_j^{ρ} is related to the open channel amplitudes by Eq. (9).

A plot of $\tau(E)$ as a function of energy for autoionization of vibrational levels of the $nd\ ^1A_1\ (^2\Sigma_g^+)$ states of NO_2 by the (000) continuum, along with a plot of the relative coefficients of the contributing closed channels, for resonances at energies up to 500 cm^{-1} above the (000) level are shown in Fig. 4. The particular calculation involves one open channel, (000), and five closed: (020), (100), (040), (120), and (200). As shown in Fig. 4, generally large widths are obtained for most of the energy levels in that region and more than one closed channel is involved in each case, as close-lying vibrational states of different n Rydberg states interact. For example, a width of 10 cm^{-1} is obtained for the (200) closed channel, interacting with the (020) channel at energy of 411 cm^{-1} above the (000) threshold. The calculated width of 10 cm^{-1} is in good agreement with the observed width of 13 cm^{-1} for the $7d\sigma$ level of NO_2.[6]

In the present work, several calculations involving the 10 channels, (000), (020), (100), (040), (120), (200), (060), (140), (220), and (300) have been carried out, using different combinations of closed and open channels in order to obtain converged results for the six lowest channels.

Figure 5 gives an overview of the spectra obtained by use of Eq. (10) in the 10-channel calculation. The energy range covers the interval between the first (000) ionization limit and the threshold for ionization of the (040) channel at 2474 cm^{-1}. Notations to the right indicate the relevant intermediate vibrational level of the $3p\sigma$ state. It is evident from the coincidence between resonance positions that there is very considerable interaction between the various closed channels, because each channel would otherwise show merely its own hydrogenlike autoionization series. The situation is particularly confused below the (020) ionization limit, where only the broad features in the (100) spectrum contains a recognizable Rydberg series. It also appears that the resonances in this channel are typically broader than those in other channels below the (020) ionization threshold, as expected from Berry's $\Delta v=1$ selection rule, although there are isolated broad features such as the resonance at 610 cm^{-1} in the (040) spectrum. We also notice a very strong feature in the (040), (120), and (200) spectra, just below the (100) ionization threshold, the possible origin of which is discussed below.

Turning to a more detailed examination of the individual spectra, Figs. 6 and 7 indicate approximate assignments determined by the channel thresholds and quantum defects derived from the diagonal elements of the K matrix, as listed in Table IV. It may be noted that the $3d\sigma$ quantum defect at the equilibrium geometry of the positive ion 0.19 (from the *ab initio* energies) is close to the values around 0.2 extracted by Campos *et al.*[6] from the observed autoionization spectra of the (100) manifold. This coincidence is to some extent fortuitous, however, because it seems unlikely that the uniform shift of all Rydberg electronic eigenvalues, to produce the correct ionization energy from the $3p\sigma$ state, will be equally

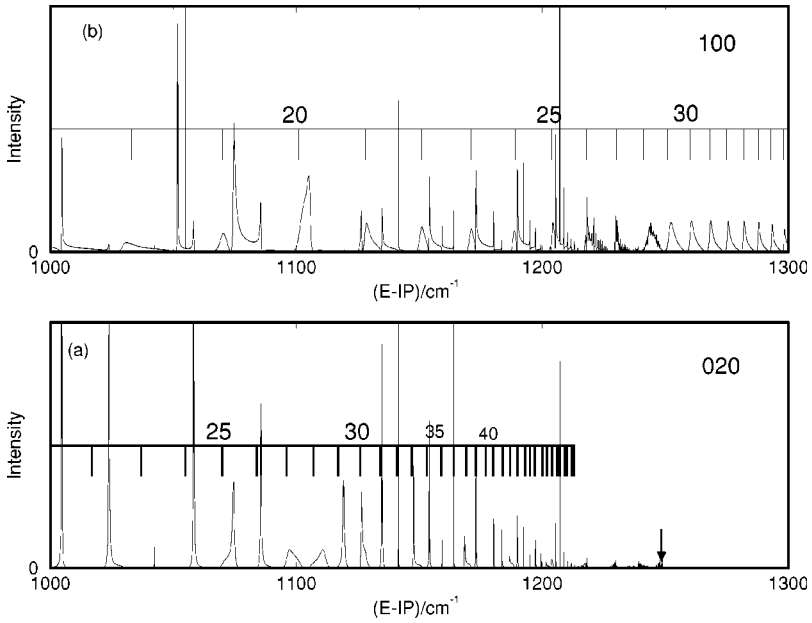

FIG. 6. Details of the spectra calculated for levels (020) and (100).

accurate for all other shifted states. The increase in the vibrationally averaged quantum defects, by between 0.06 and 0.14 units should therefore be taken primarily as a rough measure of the strength of the interchannel coupling, because the calculated off-diagonal K matrix elements are by no means uniformly smaller than the diagonal ones. It should be remembered of course, that the vibrational diagonalization in the positive ion state necessarily includes Fermi resonance coupling width in the {020,100} and {040,120,200} vibrational polyads, which adds to the stretch-bend coupling arising from mixed terms in the expansion of the quantum defect function (see Table III).

It is evident from Figs. 6 and 7 that principal quantum number assignments can be given with considerable confidence, except for the lowest levels of the (020) series, which terminates at 1250 cm^{-1}. To the extent that clear assignments are possible, the lines in the (020) series decrease broadly as n^{-3}, from 5 cm^{-1} at $n=11$ to 0.5 cm^{-1} at $n=24$ for example. Those of the (100) series are however much broader, with a width of perhaps 25 cm^{-1} at $n=11$ falling to 5 cm^{-1} at $n=24$. Notice that it is difficult to ascribe a confident width to every member of the (100) series because, for example, the complex lineshape of the $n=19$ resonance clearly arises from interaction with the $n=25$ member of the (020) series, the zeroth order position of which lies within 1 cm^{-1} of $n=19$ of (100), while $n=26$ of (020) also lies within the resonance profile. The recognition of individual peaks in the (100) series becomes progressively easier as the density of (020) resonances increases, although the line shape is far from Lorentzian. By any measure of linewidth, there is however a definite decrease from around 15 cm^{-1} at $n=12$ to 1 cm^{-1} at $n=27$, consistent with the n^{-3} law, followed by an increase to about 4 cm^{-1} at $n=28$, where the resonance lies in the quasicontinuum just below the (020) ionization thresh-

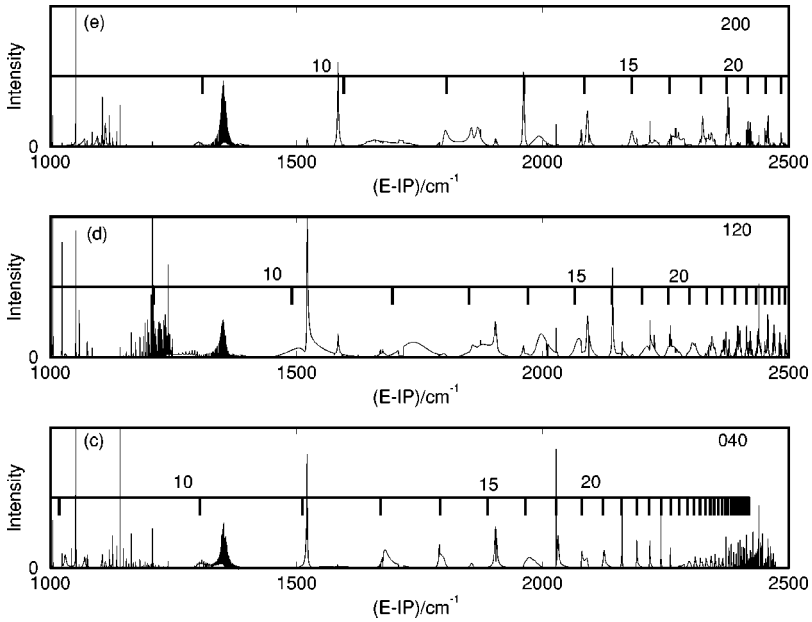

FIG. 7. Details of the spectra calculated for levels (040), (120), and (200).

TABLE IV. Channel thresholds and approximate quantum defects for the five lowest excited vibrational channels.

	020	100	040	120	200
Threshold/cm^{-1}	1250	1385	2474	2646	2769
Quantum defect	0.2735	0.3412	0.3188	0.2587	0.3281

old. This fourfold increase may be taken as a rough measure of the relative coupling strengths to the (020) and (000) continua, no doubt mediated by Fermi resonance coupling between (100) and (020), in violation of the $\Delta v=1$ coupling rule. Structure due to interaction with high levels of the (020) series disappears at the threshold, above which a sequence of smooth peaks converges on the (100) limit, apart from a major perturbation of the quasicontinuum due to interaction with $n=10$ of (040) and $n=9$ of (200) (see below).

Turning to the resonance structure in the {040,120,200} polyad in Figs. 7(c)–7(e), the strong feature at 1350 cm^{-1} is almost certainly due to a change coincidence between the $n=10$ zeroth order level of (040), the $n=9$ level of (200) and the (100) quasicontinuum, with further Fermi resonance mediated coupling to the (120) channel. The spectra at higher energies arise from autoionization to three open channels, and the increase in linewidth compared with the spectra in Figs. 6(a) and 6(b), can be attributed partly to the opening of an additional channel and partly to an increase in the magnitude of coupling matrix elements. The (200) linewidths are relatively ill-defined at low n values but they are roughly comparable to those of the (120) series for $n>15$, while the peaks in the (040) spectra are markedly sharper. For example, the $n=20$ resonance of (120) has a width of about 12 cm^{-1} compared with about 3 cm^{-1} for the (040) series, and there is nothing in the (040) spectrum to match the roughly 50 cm^{-1} width of the $n=11$ resonance of (120). The relatively slow decay of the (040) series is qualitatively in line with Berry's $\Delta v=1$ selection rule because the (120) and (200) channels can autoionize via (020) and (100) respectively, but there is no analogous route for autoionization from (040).

Campos *et al.*[6] have observed for the resonances converging to the 100 limit, widths varying between 0.2 cm^{-1} and more than 15 cm^{-1}. Generally large widths have been reported for the $nd\sigma$ states for $n=10-32$,[1] although not quite as large as those calculated in the present work: For the $n=12$ and $n=27$ levels mentioned above, the reported widths are 10.69 cm^{-1} and 0.83 cm^{-1}, respectively with the corresponding theoretical being 15 cm^{-1} and 1 cm^{-1}, respectively. Thus, there is good agreement between the observed and the calculated widths.

V. CONCLUSIONS

Potential-energy surfaces of Rydberg excited electronic states of NO_2 have been calculated by *ab initio* MRDCI calculations. Significant valence-Rydberg interactions at nonlinear geometries complicate the shapes of the potential-energy surfaces of most of the Rydberg states. Single-channel quantum defect function were obtained for the $nd\sigma$ states and vibrational autoionization spectra from the $nd\sigma$ states via double resonance excitation via several vibrational levels of the $3p\sigma$ state were calculated. Significant interchannel coupling was observed, particularly for low n states, but recognizable autoionization series could be recognized for $n>15$. Trends in the autoionization linewidths conformed roughly to Berry's $\Delta v=1$ selection rule, but with some exceptions attributable to Fermi resonance coupling. A typical linewidth decrease as n^{-3} in a given series was also observed.

[1] W. A. Chupka and E. R. Grant, J. Phys. Chem. A **103**, 6127 (1999).
[2] H. Matsui, J. M. Behm, and E. R. Grant, J. Phys. Chem. **101**, 6717 (1997).
[3] E. Mayer, E. Zückerman, L. Zhang, H. Hedderich, J. Behm, and E. Grant, Philos. Trans. R. Soc. London, Ser. A **355**, 1569 (1997).
[4] H. Matsui and E. R. Grant, J. Chem. Phys. **104**, 42 (1996).
[5] G. Bryant, Y. Jiang, M. Martin, and E. R. Grant, J. Chem. Phys. **101**, 7199 (1994).
[6] F. X. Campos, Y. Jiang, and E. R. Grant, J. Chem. Phys. **94**, 5897 (1991); **93**, 2308 (1990).
[7] M. B. Knickelbein, K. S. Haber, L. Bigio, and E. R. Grant, Chem. Phys. Lett. **131**, 51 (1986); L. Bigio, R. S. Tapper, and E. R. Grant, J. Phys. Chem. **88**, 1271 (1984).
[8] Ch. Jungen and S. T. Pratt, J. Chem. Phys. **106**, 9529 (1997).
[9] F. Châteauneuf and H. Lefebvre-Brion, J. Chem. Phys. **98**, 7657 (1993).
[10] I. D. Petsalakis, G. Theodorakopoulos, and M. S. Child, J. Phys. B **28**, 5179 (1995).
[11] G. Theodorakopoulos, I. D. Petsalakis, and M. S. Child, J. Phys. B **29**, 4543 (1996).
[12] G. Herzberg, *Electronic Spectra of Polyatomic Molecules* (Van Nostrand, New York, 1966).
[13] G. Gillispie, A. U. Khan, A. C. Wahl, R. P. Hosteny, and M. Kraus, J. Chem. Phys. **63**, 3425 (1975).
[14] C. F. Jackels and E. R. Davidson, J. Chem. Phys. **65**, 2941 (1976).
[15] S.-K. Shih, S. D. Peyerimhoff, and R. J. Buenker, Chem. Phys. Lett. **46**, 201 (1977).
[16] R. J. Buenker, *Studies in Physical and Theoretical Chemistry: Current Aspects of Quantum Chemistry 1981*, edited by R. Carbo (Elsevier, Amsterdam, 1982), Vol. 2, p. 17.
[17] R. J. Buenker and R. A. Phillips, J. Mol. Struct.: THEOCHEM **123**, 291 (1985).
[18] G. Theodorakopoulos, I. D. Petsalakis, and M. S. Child, J. Mol. Struct.: THEOCHEM **434**, 177 (1998).
[19] T. H. Dunning, J. Chem. Phys. **55**, 716 (1971).
[20] C. H. Greene and Ch. Jungen, Adv. At. Mol. Phys. **21**, 51 (1985).
[21] S. C. Ross, *Proceedings of the AIP Conference 225 Half-collision Resonance Phenomena in Molecules* (Caracas, Venezuela, 1990), p. 78.